High Temperature Corrosion of Materials
https://doi.org/10.1007/s11085-024-10257-8

ORIGINAL PAPER

Novel Chromium–Silicon Slurry Coatings for Hot Corrosion Environments

M. Kerbstadt[1] · K. Ma[2] · E. M. H. White[1] · A. J. Knowles[2] · M. C. Galetz[1]

Received: 5 July 2024 / Revised: 5 July 2024 / Accepted: 17 July 2024

Abstract

Ni-based superalloys are commonly used in gas turbines because of their exceptional high-temperature mechanical properties. To secure a long service life, the materials must also have sufficient corrosion resistance. Therefore, diffusion coatings are widely used to enrich the surface in protective oxide scale-forming elements. For temperatures between 650 and 950 °C, where hot corrosion occurs, Cr-based coatings are advantageous. These are commonly applied via the laborious pack cementation process. Recently, a novel cost-effective Cr/Si slurry coating process has been developed which demonstrated resistance to oxidative high-temperature environments. Here, the protection of the slurry coatings against hot corrosion type I at 900 °C on the Ni-based superalloy Rene 80 is investigated and compared to coatings produced by pack cementation. Prior to the 300-h exposures in air containing 0.1% SO_2 at 900 °C, 4 mg/cm^2 of Na_2SO_4 was deposited on the material surfaces. The uncoated Rene 80 exhibited rapid dissolution of the initial oxide scale followed by catastrophic break away oxidation. In comparison, the slurry coatings showed significantly improved hot corrosion resistance compared to the uncoated alloy and a better protection than a Cr pack cementation coating. The Cr pack cemented Rene 80 showed improved hot corrosion resistance, but Cr depletion in the subsurface zone occurred with increasing exposure time, associated with the propagation of Al internal oxidation and increasing sulfidation. In contrast, the slurry coatings formed an external Cr_2O_3 scale coupled with an agglomeration of SiO_2 underneath and a continuous Al_2O_3 subscale which offered a better diffusion barrier and leading to superior long-term protection against hot corrosion.

Keywords Diffusion coatings · Chromium slurry coating · Chromium–silicon coating · Hot corrosion type I

✉ M. Kerbstadt
michael.kerbstadt@dechema.de

[1] DECHEMA-Forschungsinstitut, Frankfurt am Main, 60486 Frankfurt, Germany

[2] School of Metallurgy and Materials, University of Birmingham, Birmingham B15 2TT, UK

Published online: 24 July 2024

Introduction

Ni-based superalloys are widely used as materials for hot sections of gas turbines. As the materials are applied in a combustion environment and therefore exposed to hot and aggressive gases, high-temperature corrosion and oxidation resistance is required. At sufficient partial pressure of SO_2/SO_3, components can degrade due to hot corrosion. Hot corrosion is induced by the deposition of thin salt films, most commonly sodium sulfate (Na_2SO_4) [1]. Deposition of Na_2SO_4 can occur from the reaction of NaCl from seawater with sulfur oxides from sulfur-containing fuels [2] or air pollution. Na_2SO_4 melts at lower temperatures ($T_m = 884$ °C [3]) and can then react with the oxides of the material to dissolve via an acid–base reaction [4]. Hot corrosion of Ni-based alloys by (Na_2SO_4) can be divided into two regimes: type II at temperatures of 500–700 °C where the salt forms low melting eutectics (i.e., Na_2SO_4–$NiSO_4$ at 671 °C) and type I at 800–950 °C, where Na_2SO_4 melts directly and can dissolve the oxide scales without an incubation period [5]. With increasing temperature, the P_{SO3} decreases in favor of P_{SO2}, shifting the salt activity from Na_2SO_4 to Na_2O [5]. As a result, a basic dissolution becomes more likely, especially when sulfur and oxygen are also consumed by the corrosion reactions. Hot corrosion attack can be mitigated by protective oxide scales which exhibit a low solubility in Na_2SO_4 [6]. In general, the presence of a liquid Na_2SO_4 deposit shortens the time during which protective scales can form by selective oxidation due to continuous depletion, thus accelerating the corrosion attack [7, 8]. To counteract this and create a sufficient reservoir to form protective scales (of Al, Cr and/or Si), diffusion coatings are commonly applied [9, 10]. Cr-modified Al coatings or Cr-based coatings favor thermodynamically highly stable chromium sulfides, binding sulfur and preventing inward diffusion [6, 11]. Furthermore, Cr_2O_3 exhibits advantageous behavior by limiting the basicity of the melt when dissolved in Na_2SO_4. In contrast to other oxides, it has lower solubility at lower oxygen partial pressures. Thus, it reprecipitates at the oxide/metal interface and slows down the corrosion process [12].

The state-of-the-art and industrially used process for chromizing is pack cementation [2]. In pack cementation the coating deposition occurs via a CVD process. The components are usually fully embedded in a powder mixture which contains the metallic source, filler material (usually Al_2O_3) and a halogenide activator. During the heat treatment, the halogenide reacts with the metallic element from the source and transports it to the substrate surface via the gas phase where the metal source diffuses into the material [9, 13, 14]. However, such a coating process presents limitation in costs as it requires a large quantity of powders to embed the components. An alternative and simpler process is a slurry coating, which has been already well established and widely used for Al-based coatings [15, 16]. The metal powder is mixed with a binder liquid into a slurry which is deposited on the substrate surface. During the post-heat treatment, the coating forms via interdiffusion between the powder particles and the substrate surface. The existence of a liquid phase is necessary to reach sufficient diffusion rates and form a thick enough diffusion zone [9], reducing time and cost. Because of the

melting point of Cr above 1900 °C, the development of a comparable slurry process to Al-based coatings for Cr-based coatings has been challenging.

A new and environmentally friendly process to apply Cr/Si-based slurry coatings has recently been patented, and demonstrated [17, 18]. Under air at 900 °C, the coatings with high Cr contents up to a depth of 150 µm improved the oxidation resistance of Inconel 740H and Rene 80, due to the combination of a Si-rich subscale underneath a slow-growing Cr_2O_3 scale. Here we performed a systematic study of the hot corrosion behavior of uncoated, Cr pack cemented and Cr/Si slurry-coated Rene 80 to reveal and highlight the protective effects from the coatings.

Experimental Procedures

The Cr/Si slurry coatings and pack cementation coatings were applied on the Ni-based superalloy Rene 80 [19]. The nominal composition of Rene 80 is given in Table 1. Samples were cut into a planar geometry of (20×10×2) mm using electrodischarge machining (EDM). The procedure of the Cr/Si slurry coating was briefly aforementioned above and is described in detail in [18]. Prior to coating, both pack cementation and slurry-coated samples were sand-blasted and cleaned in an ethanol ultrasonic bath. For pack cementation, the samples were embedded into a powder mixture inside an Al_2O_3 crucible. The powder contained 5 wt.-% Cr powder as the metallic source, 2 wt.% $MnCl_2$ powder as activator and 93 wt.% Al_2O_3 powder as filler material. The heat treatment was carried out at 1050 °C for 4 h at a gas flow of 5 l/h of Ar-5vol.% H_2 in a quartz tube furnace. After coating application, all samples were ground to P1200 to remove any remaining uneven surface residue prior to the exposure tests. Before the Na_2SO_4 deposition, Na_2SO_4 powder (≥99% granular, Alfa Aesar, Haverhill, MA, USA) was dissolved in distilled water and the solution sprayed by an airbrush to distribute the salt evenly. During the deposition, the samples were placed on a heating plate at ~ 80 °C. A total amount of ~ 4 mg/cm^2 of salt was deposited and monitored by weighing of the samples.

The quasi-isothermal (24, 100, 300 h) exposures were carried out in a 20-cm-diameter quartz tube furnace at 900 °C under a calibrated gas flow of 75 ml/min of 0.9 vol. % synthetic air and 0.1 vol.-% SO_2. After each time step, a sample of each type was removed and cross-sectioned using standard metallographic techniques. Due to overlapping effects of scale growth, internal damage, spallation of corrosion products and salt along the edges of the samples, the metal loss or the corrosion depth measured based on the cross-sectional reduction is a more suitable way to assess the corrosion progress [20–22]. Six optical images throughout each sample were taken with a magnification of 50x (LEICA DMC 450). The remaining metal thickness was determined by averaging six perpendicular length measurements in each image using ImageJ software. The

Table 1 Nominal chemical compositions in wt.% of Rene 80

Cr	Co	Al	Ti	Mo	W	C	Hf	B	Zr
14	9.5	3	5	4	4	0.17	0.03	0.02	0.03

measurement began below the visible corrosion zone with internal damage in order to determine the remaining "good" metal.

Samples were characterized using scanning electron microscopy (SEM, Hitachi FlexSEM 1000 and Thermo Scientific Apreo 2 SEM), electron probe microanalysis (EPMA, JEOL JXA-8100) equipped with wavelength dispersive X-ray spectroscopy (WDS) and X-ray diffraction (XRD, Bruker D8 XRD Advance with Cu-Kα source). Back-scattered electron (BSE) images were taken using SEM to reveal the microstructures. One slurry-coated sample after hot corrosion for 300 h at 900 °C was analyzed using transmission electron microscopy (TEM). The TEM lamella lift-out was prepared by focus ion beam (FIB) equipped on an FEI Quanta 3D field emission gun (FEG) dual-beam SEM. TEM and scanning TEM (STEM) combined with energy-dispersive X-ray spectroscopy (EDS) were performed using a Tecnai F20 at 200 kV equipped with Oxford INCA EDS instrument. The measurements included EDS point measurements and element distribution maps. The identification and assumption of the phases present were performed based on the measured compositions within the WDS line scans and crystallography, correlating with existing phases in the PDF2 database as well as by calculations using the JMatPro-v10.2 software.

Results and Discussion

Microstructure of Coated Rene 80

A representative as-coated cross section and concentration profile of a pack cementation chromized Rene 80 is shown in Fig. 1. On the surface, a characteristic ~ 2 µm thick layer of $Cr_{23}C_6$ (confirmed by XRD, pdf2 file number used: 00–035-0783, not shown here) formed [13, 23, 24]. The high Cr activity from the deposition of an initial pure Cr layer on the material surface and a sufficiently high C activity from the C contained in Rene 80 enable the formation of the $Cr_{23}C_6$ layer, as shown before for other substrates [25]. Below the $Cr_{23}C_6$, the γ-Ni layer is enriched by up to 28 at.-% Cr which decreases until the nominal composition of Rene 80 is reached

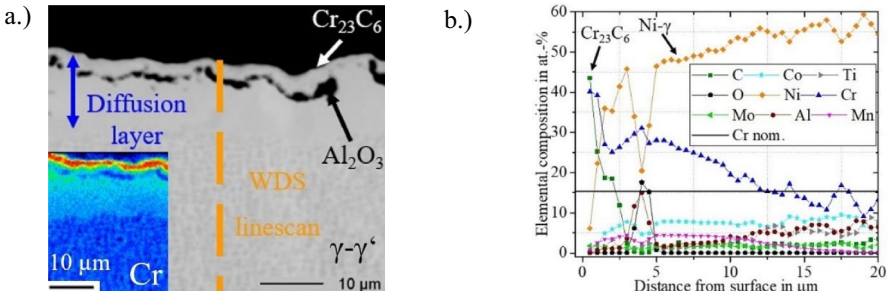

Fig. 1 Pack cementation Cr-coated Rene 80: **a** SEM cross-section; **b** concentration depth profiles measured by WDS

after ~ 15 µm, where the transition to the γ-γ'-microstructure occurs. Below the $Cr_{23}C_6$ layer inclusions of Al_2O_3 formed. This can be attributed to Kirkendall porosity by outward diffusion, which was then filled by Al_2O_3 during the heat treatment due to the Al content in Rene 80. An enrichment of Mn from the $MnCl_4$ activator used up to 4.5 at.% within the diffusion layer is visible, but a significant incorporation of Cl could not be detected.

Characterization of the Cr/Si slurry-coated Rene 80 is described in detail in [18], and a representative as-coated cross section and concentration profile is shown in Fig. 2. The thickness of the diffusion layer and therefore the incorporated Cr reservoir is ~ 10 times larger for the Cr/Si slurry coating. The coating consists of a Cr- and Si-enriched γ-Ni matrix with precipitates of coarsened Si-rich M_6C carbides and locally fine Ti-enriched MC carbides along the grain boundaries. The Cr content is at a maximum of 28 at.% in the outer zone of the diffusion layer and continuously decreases within ~ 150 µm, where the nominal composition of Rene 80 is approached.

In the pack cementation process, deposition occurs via gaseous Cr, while during the slurry process a Cr-containing liquid phase is created. The activity is expected to be significantly higher in the partially molten state, resulting in higher interdiffusion rates and a thicker diffusion layer. In addition, the $Cr_{23}C_6$ layer initially forms during the pack cementation process, which serves as a diffusion barrier, limiting the diffusion and thus the further enrichment of the surface with Cr [13]. With this novel slurry process, no $Cr_{23}C_6$ layer formed. Also, Harper et al. [26] reported the absence of a $Cr_{23}C_6$ layer during co-deposition of Cr and Si by the pack cementation process. Whether this is an effect of the addition of Si or the different application process cannot be conclusively assessed based on the results in the present work. However, it can be assumed that due to the initial concentration of $Cr_{50}Ni_{30}Si_{20}$ in the slurry powder as well as the immediate melting, the C and Cr activities required for the formation of $Cr_{23}C_6$ on the surface are not sufficient.

Hot Corrosion Behavior

In Fig. 3a the measured metal loss from the analysis of the various cross sections due to hot corrosion is shown. The uncoated Rene 80 shows a huge average metal

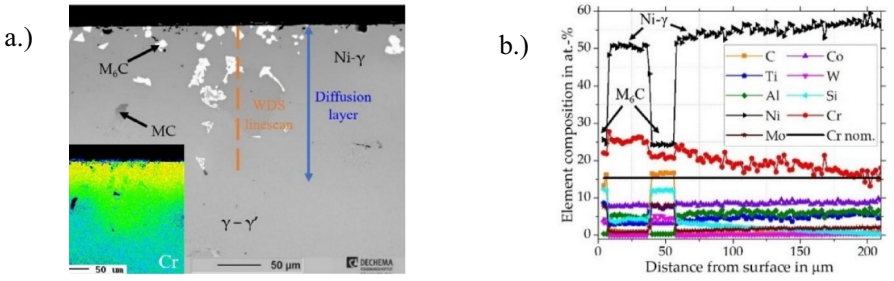

Fig. 2 Cr/Si-coated Rene 80 after [18]: **a** SEM cross section; **b** concentration depth profiles measured by WDS

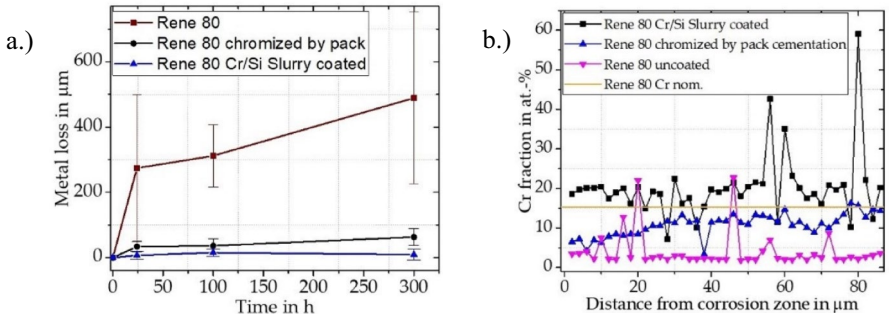

Fig. 3 **a** Metal loss from cross section analysis over time during hot corrosion at 900 °C; **b** Cr depletion after 300 h of exposure

loss of 470 µm after 300 h, while the Cr pack cementation and Cr/Si slurry coatings show a loss below 80 µm. A reduction of > 0.5 mm by metal loss is an unacceptable reduction of load-bearing cross section in actual parts. Additionally, after 300 h, the Cr content below the corrosion zone was determined to indicate whether breakaway oxidation is imminent and to what extent the reservoir has been consumed. While Cr depletion is apparent for the uncoated and pack cementation-coated Rene 80 up to 80 µm, the subsurface region of the Cr/Si coating maintains a reservoir of ~ 20 at.% Cr (Fig. 3b).

Uncoated Rene 80

In Fig. 4 a cross section of uncoated Rene 80 with corresponding elemental distribution maps after 24 h of exposure is shown. Breakaway oxidation was accompanied by extensive internal oxidation and sulfidation. The present corrosion attack indicates rapid dissolution of the initially formed Cr_2O_3 scale by the molten Na_2SO_4, followed by continuous breakdown of the scale and S uptake into the alloy, which leads to extensive internal sulfidation. Because of the relatively low SO_3 activities at 900 °C, basic dissolution of the oxides can be expected [5], where Cr_2O_3 scales would usually not be expected to demonstrate continuous self-sustaining hot corrosion

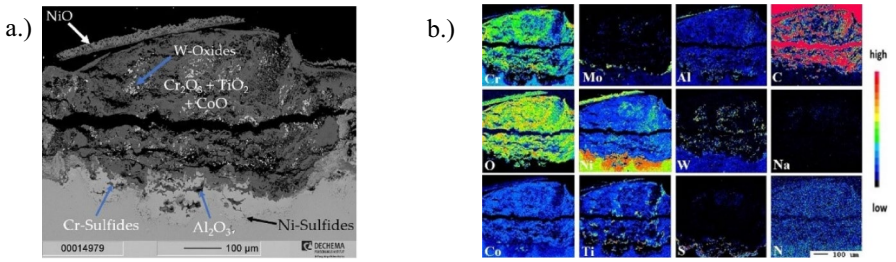

Fig. 4 Characterization of uncoated Rene 80 after 24 h at 900 °C: **a** SEM BSE image; **b** EPMA maps of major elements

attack [12]. However, Rene 80 is comparatively highly alloyed with refractory Mo and W for mechanical stability [27, 28]. Mo and W form very acidic oxides, and when these are dissolved in the molten salt, they strongly reduce the Na_2O activity. This makes the salt locally very acidic, which can lead to the acidic dissolution and increase of solubility of Cr_2O_3 in Na_2O [11, 29, 30]. The incorporation of W-oxides within the corrosion products is visible in Fig. 4, while Mo-oxides have probably evaporated [11]. It was reported that especially high Mo content, up to 4 wt.-% (such as Rene 80), can accelerate hot corrosion attack at 900 °C [31] because of the high acidity of this oxide.

After depletion of Cr, Ni is oxidized and reacts with the molten Na_2SO_4. It reprecipitates as the observed outer porous and unprotective NiO scale [11]. This had spalled off in Fig. 3, but was still attached in other areas of the sample. Below the corrosion front an inward-growing blister formed, which is a common shape of attack for hot corrosion type I and is already considered catastrophic corrosion [32]. At the interface, the alloying elements such as Ti and Al are selectively oxidized, causing a dissolution of the Ti- and Al-rich γ' Ni_3(Ti,Al) (Fig. 3b).

Due to the lack of a protective oxide layer, S from the SO_2-containing gas quickly diffused into the alloy and led to extensive internal sulfidation. Ni sulfides and Cr sulfides could be identified by EDS point measurements (not shown). Thermodynamically Ni sulfides are less stable when compared to Cr sulfides and Ti sulfides [33]. Based on exposures of Rene 80 at 1050 °C in air-2%SO_2, Jalowicka et al. [34] concluded that first Ti sulfides form and after longer exposure times additional Cr sulfides form due to the reduced Ti activity by subsequent depletion and further transformation into Ti oxide. The additional Na_2SO_4 deposit accelerates the depletion of Ti and Cr, so that Ni sulfides were formed. As the corrosion progressed and the porous corrosion products on the surface spalled, all sulfides are oxidized and the released sulfur diffuses further into the alloy. Particularly, the existence of Ni sulfides (liquid under these conditions) accelerates the progression of the corrosion front [5].

Chromized Rene 80 by Pack Cementation

The pack cementation Cr-coated Rene 80 showed considerably slower and reduced corrosion attack when compared to the uncoated Rene 80, as indicated by the lower metal loss in Fig. 3. A cross section with corresponding elemental maps after 24 h is shown in Fig. 5. The initially formed Cr_2O_3 scale layer appears to have spalled off, which was evident by the spalled material in the crucible. Another indication that spalling occurred during the exposure is the pronounced surface porosity within the subsurface zone, which filled with resin during embedding of the samples and is visible as C-rich locations in the elemental map in Fig. 4b. It is known that Mn additions potentially increase the growth rates of Cr_2O_3 scales due to the simultaneous formation of $MnCr_2O_4$ spinel and, therefore, make the oxides more susceptible to spalling [35]. Since Mn is no longer visible in the EPMA maps in Fig. 5b after 24 h of exposure, Mn appears to have been enriched in the scale and promoted spalling. Due to the Cr reservoir,

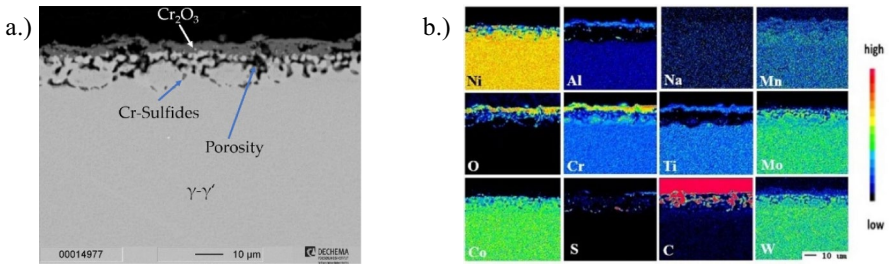

Fig. 5 Pack cementation Cr-coated Rene 80 after 24 h at 900 °C: **a** SEM BSE image; **b** EPMA elemental distribution maps of major elements

a self-healing of Cr_2O_3 was possible where Cr diffused outward and resulted in the observed Kirkendall porosity. After 24 h, a Cr reservoir remained, although it was significantly reduced and within 8 µm of the surface returned to a composition of ~ 18 at.-% Cr (measured by WDS). No remaining Cr-rich $Cr_{23}C_6$ phase is evident. Locally some S diffused inward and formed Cr sulfides, thus also contributing to Cr depletion. As Cr sulfide compounds are stable and trap S, further diffusion into the alloy is slowed down.

In Fig. 6 a cross section with the corresponding elemental maps after 300 h of exposure is shown. A dense Cr_2O_3 scale developed with a TiO_2 scale at the metal/scale interface. TiO_2 precipitates within the outer part of the Cr_2O_3 scale are also evident. Below the oxide scales is a growing zone of internal oxidation of Al (to Al_2O_3). Since the initially formed porosity disappears, it is likely that it filled with Al_2O_3. Underneath the oxidation zone, where the oxygen partial pressure is reduced, a zone of Cr sulfides and TiN (confirmed by EDS point measurements) formed. The Cr reservoir is completely used up after 300 h, and within the depletion zone of ~ 50 µm, the Cr content is reduced to below 8 at.-% within the first ~ 20 µm. No additional sulfides beyond Cr sulfides could be identified. However, with further depletion, the formation of detrimental nickel sulfides is expected. If salt deposits repeatedly occur and the Cr_2O_3 scale dissolves again, catastrophic breakaway oxidation would occur within a short period of time.

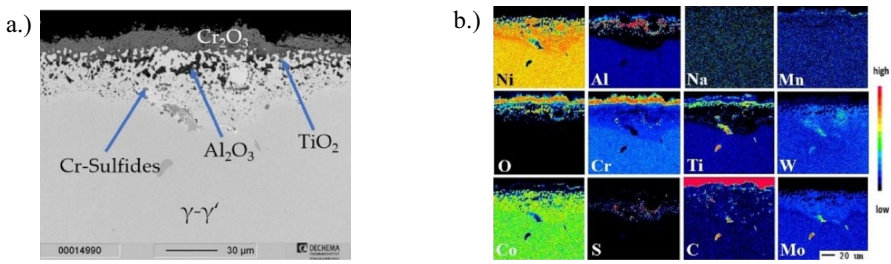

Fig. 6 Pack cementation Cr-coated Rene 80 after 300 h at 900 °C: **a** SEM BSE image; **b** EPMA maps of major elements

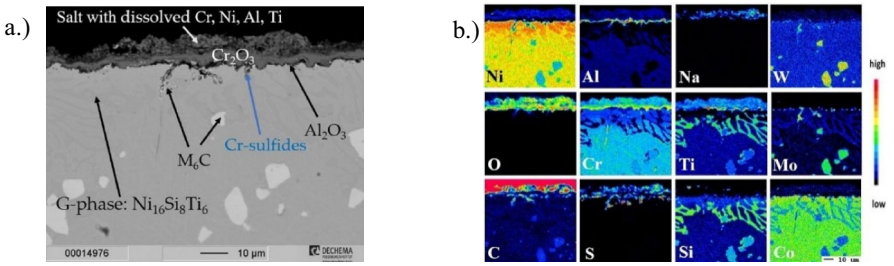

Fig. 7 Cr/Si slurry-coated Rene 80 after 24 h at 900 °C: **a** SEM BSE image; **b** EPMA maps of major elements

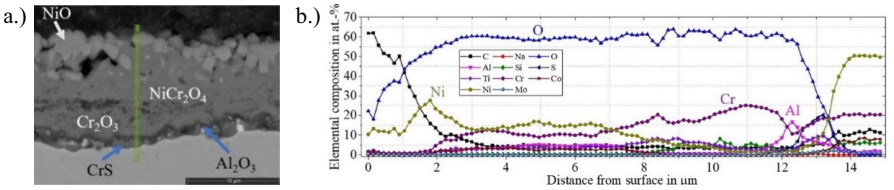

Fig. 8 Cr/Si slurry-coated Rene 80 after 100 h at 900 °C: **a** SEM BSE image; **b** EDS profile, along line marked in (**a**)

Cr/Si Slurry-Coated Rene 80

Figure 7 presents a BSE image of a Cr/Si-coated sample after 24 h of exposure. An external porous layer containing Ni, Cr, Ti, Al, O, S and Na (Fig. 7b) indicates that these are reaction products from the molten Na_2SO_4, which seems to have partly dissolved the initial Cr_2O_3 scale. Below this porous layer is a Cr_2O_3 scale with a continuous Al_2O_3 subscale. No large-scale corrosion attack and uptake of S into the material is evident. The partial dissolution of the oxide scale and subsequent outward diffusion of Cr to maintain scale growth led to a depletion of Cr within ~ 10 µm, where the Cr content of ~ 14 at.-% was measured (by WDS, approx. the base composition of the alloy). However, underneath the thin depletion zone a ~ 150 µm Cr reservoir is present, with a Cr content of at least 20 at.-%. Within the Cr depletion zone, a Si- and Ti–rich phase precipitated. According to thermodynamic calculations (JMatPro, not shown here) and from the given phase compositions in [36], this phase can be assumed to be cubic $Ni_{16}Si_8Ti_6$.

Figure 8 shows a BSE image with a corresponding EDS line scan of the corrosion zone after 100 h. In the outer part of the oxide scale NiO precipitation within a $NiCr_2O_4$ matrix (confirmed by XRD pdf2 file number used: 00-075-0198 with the spinel structure) is evident. Progressing inward, the Cr content increases and a ~ 3 µm thick Cr_2O_3 scale can be measured (Fig. 8b). The structure of the oxide layers indicates that the partial dissolution of the oxide scale occurred by the basic fluxing mechanism. The oxides are dissolved by the molten Na_2SO_4 at the salt/oxide interface and reprecipitate according to their solubility gradient at a specific location within the melt. Since NiO shows a negative solubility gradient within the molten

Na_2SO_4, it reprecipitates within the outer parts of the melt where the oxygen partial pressure is increased [12], as shown in Fig. 8a. In contrast to NiO, Cr_2O_3 shows a positive solubility gradient within the molten Na_2SO_4. Solubility of Cr_2O_3 increases with increasing oxygen partial pressure and therefore reprecipitation occurs at the oxide/salt interface [12]. This inhibiting behavior can be seen by the increasing Cr content within the oxide products in Fig. 7. For high Cr concentrations, like for the investigated Cr/Si slurry coating, the dissolution process slows down and is not self-sustained.

Where M_6C precipitates are at the surface, these are oxidized and allow S uptake, as the formation of Ti sulfides can be seen at these locations. Mo- and W-rich carbides at the surface represent potential locations for increased corrosion due to their preferential oxidation and the local change of salt acidity by these oxides [11, 37]. However, the Cr/Si slurry coating effectively inhibits the attack and appears to hinder the spreading of the corrosion front.

After 300 h of exposure in Fig. 9, the microstructure is similar to the one after 100 h. After formation of the multilayer oxide scale, the corrosion process seems to follow steady state behavior. This is also supported by the recorded metal loss in Fig. 3. A TEM image of the interface between the oxide layer and metal is shown in Fig. 9 with the corresponding EDS maps. The presence of Ni in the oxide is limited to the outer region. Close to the interface between the Cr_2O_3 and the Al_2O_3 scale, an agglomeration of Si-rich precipitates was confirmed by STEM-EDS to be SiO_2 which is most likely amorphous [38, 39]. Due to the decreased oxygen partial pressure from Cr_2O_3, Si is oxidized and forms SiO_2 precipitates at the Cr_2O_3/metal interface according to Wagner's getter mechanism [40]. With the coating containing ~ 5 at.% Si, it could be expected that the SiO_2 particles would agglomerate over time to a dense subscale, as observed in [18, 38, 41]. Here, below the SiO_2 particles Al_2O_3 formation is found. Under the current conditions, even the formation of a dense Al_2O_3 film becomes possible, most likely due to the "support" from SiO_2 in lowering the oxygen partial pressure, although the discrete influence of the agglomerated

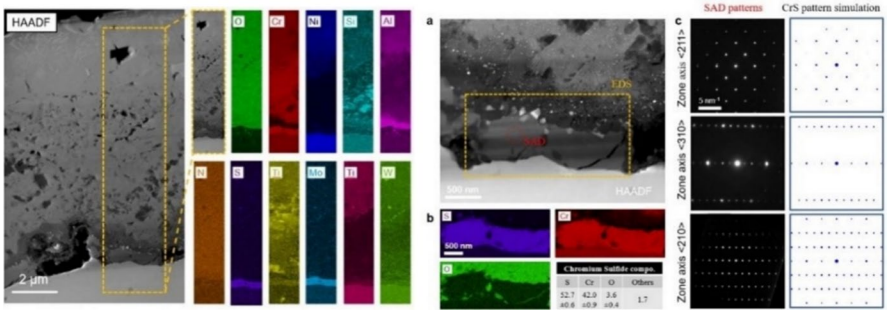

Fig. 9 TEM characterization of Cr/Si slurry-coated Rene 80 after 300 h at 900 °C. Left: Image with EDS maps. Right: Characterization of Cr sulfide. **a** STEM high angle annual dark field image. **b** STEM/EDS distribution of S, Cr and O. **c** Selected area diffraction (SAD) patterns of Cr sulfide acquired along < 211 >, < 310 >, and < 210 > zone axes compared with the simulated patterns. The lattice parameters used for simulation are $a = 3.487$ Å, $b = 3.487$ Å, $c = 5.5278$ Å, $\alpha = 90°$, $\beta = 90°$, $\gamma = 120°$, space group P 63/m m c

SiO_2 particles on the corrosion behavior cannot be conclusively assessed within the current study. However, one effect appears to be suppression of local, unprotective, internally oxidized Al_2O_3, as seen for the Cr_2O_3 scale formed after pack cementation. Afterward, in the Si-modified slurry coating, the Al_2O_3 subscale drastically slows down further potential outward diffusion of other elements.

In general, Al_2O_3 scales are known to be more effective diffusion barriers against O and S than Cr_2O_3 [33] and the subsequent oxidation and sulfidation of the Cr/Si slurry-coated Rene 80 was hindered by the continuous Al_2O_3 scale once it formed [5]. Sheybany and Douglass [42] reported rapid sulfidation for Cr_2O_3-forming alloys, while Al_2O_3-formers showed several orders of magnitude lower S uptake. Due to the local reduction in the oxygen partial pressure and increase in sulfur activity at the interface, the sulfides become more stable than the corresponding oxides [43]. The CrS film (confirmed by TEM in Fig. 8) instead of Cr_2S_3 and the precipitation directly underneath the Al_2O_3 subscale underline the prevailing low sulfur partial pressure. The Cr depletion below the oxidation zone also became less pronounced. As the presence of silicon is known to increase the diffusivity of Cr [44], most likely the Si additions had a beneficial effect in this reduction. As a result, also the previously precipitated $Ni_{16}Si_8Ti_6$ phase dissolved. A Si depletion within the subsurface zone or diffusion of Si into the substrate could not be detected within the exposure time of 300 h, as the WDS measured Si content in the diffusion layer after exposure is comparable to the Si content in the as-coated state.

The Cr enrichment of the Cr/Si slurry enabled formation of stable CrS and reduced S-inward diffusion by the Al_2O_3 layer prevented internal sulfidation, in contrast to the single Cr_2O_3 layer of the pack cementation. The existing protective multiscale oxide layer and the remaining Cr reservoir after 300 h of exposure indicate that the protective effect of the coating would be retained even after longer exposure times or repeated Na_2SO_4 deposition.

Summary and Conclusions

The type I hot corrosion behavior of Rene 80 was investigated and compared to the results of chromized Rene 80 by the conventional pack cementation process and the recently developed Cr/Si slurry process. The uncoated Rene 80 showed rapid dissolution of the initial oxide scale, which led to breakaway oxidation with massive internal sulfidation throughout the sample within the first 24 h of exposure. Although the pack cementation Cr-coated Rene 80 showed extensive spalling of the oxide scale within the first 24 h, the Cr reservoir enabled healing of the Cr_3O_2 scale. With further exposure Cr depletion of the subsurface, internal oxidation of Al_2O_3 and a 30 µm zone of extensive internal sulfidation (stable Cr sulfides) could be observed. The pack cementation Cr coating significantly increased the hot corrosion resistance of Rene 80 and avoided catastrophic breakaway oxidation within 300 h. Nevertheless, with increasing duration and repeated salt deposition, catastrophic corrosion attack could be expected due to eventual Cr depletion.

The Cr/Si slurry-coated Rene 80 showed excellent type I hot corrosion resistance. Basic fluxing of the oxide scale could be inhibited by the protective reprecipitation

of Cr_2O_3 along the oxide/salt interface. Due to the Si content present in the coating, agglomerated SiO_2 particles formed underneath, which is believed to lead to a significant decrease of the inward diffusing oxygen, enabling the formation of a dense Al_2O_3 subscale. The resulting multilayer oxide scale represents an excellent diffusion barrier to O and S. Thus, instead of S uptake and internal sulfidation, the inwardly diffused sulfur was bound directly at the oxide/metal interface in the form of a stable CrS film.

Acknowledgements This project has received funding from the European Union's Horizon 2020 Research and Innovation Action (RIA) under grant agreement No. 958418 (COMPASsCO2). A Knowles acknowledges support from: UKRI Future Leaders Fellowship (MR/ T019174/1) and Royal Academy of Engineering Research Fellowship (RF\201819\18\158). The authors would like to thank G. Schmidt for EPMA analysis, C. Oskay for the support with pack cementation and the Centre for Electron Microscopy (University of Birmingham) for their support and assistance in this work.

Author Contributions M.K. contributed to conceptualization, methodology, investigation, and writing of the main manuscript text; K.M. contributed to TEM and SEM analysis, preparation of Figs. 8 and 9, and review and editing; E.M.H.W contributed to conceptualization, writing—review and editing, and supervision; A.J.K. performed review and editing and funding acquisition; M.C.G. contributed to conceptualization, writing—review and editing, supervision, project administration, and funding acquisition. All authors reviewed the manuscript.

Funding Open Access funding enabled and organized by Projekt DEAL. European Union's Horizon 2020 Research and Innovation Action (RIA), No. 958418 (COMPASsCO2), No. 958418 (COMPASsCO2), No. 958418 (COMPASsCO2), No. 958418 (COMPASsCO2), No. 958418 (COMPASsCO2), UKRI Future Leaders Fellowship, MR/ T019174/1,MR/ T019174/1, Royal Academy of Engineering Research Fellowship, (RF\201819\18\158), (RF\201819\18\158).

Data Availability No datasets were generated or analyzed during the current study.

Declarations

Conflict of interest The authors declare no competing interests.

References

1. F. S. Pettit, *Oxidation of Metals* **76**, 1 (2011).
2. G. W. Goward, *Surface and Coatings Technology* **108**, 73 (1998).
3. P. Kofstad and G. Åkesson, *Oxidation of Metals* **14**, 301 (1980).
4. J. Stringer, *Materials Science and Technology* **3**, 482 (1987).
5. H. J. Maier, T. Niendorf, and R. Bürgel, *Handbuch Hochtemperatur-Werkstofftechnik*, (Springer-Verlag, Wiesbaden, 2015).
6. R. Bianco, R. A. Rapp, and J. L. Smialek, *JoES* **140**, 1191 (1993).

7. F. S. Pettit, G. H. Meier, M. Gell, et al., *Superalloys* **85**, 651 (1984).
8. N. Birks, G. H. Meier, and F. S. Pettit, *JoM* **39**, 28 (1987).
9. M. C. Galetz, in *Superalloys*, ed. M. Aliofkhazraei (InTechOpen, London, UK, 2015), p. 277.
10. P. Kofstad, *Materials Science Forum* **154**, 99 (1994).
11. J. A. Goebel, F. S. Pettit, and G. W. Goward, *Metallurgical Transactions* **4**, 261 (1973).
12. R. A. Rapp and N. Otsuka, *ECST* **16**, 271 (2009).
13. R. Bianco and R. A. Rapp, *Metallurgical and Ceramic Protective Coatings*, (Springer, Netherlands, Dordrecht, 1996), p. 236.
14. J. R. Nicholls, *JoM* **52**, 28 (2000).
15. B. Grégoire, G. Bonnet, and F. Pedraza, *Surface and Coatings Technology* **374**, 521 (2019).
16. X. Montero, M. C. Galetz, and M. Schütze, *JOM* **67**, 77 (2015).
17. M. Kerbstadt, M. C. Galetz, Verfahren zur diffusionsbeschichtung mit einem Cr-Si-haltigen Schlicker. Germany Patent 10 2022 112 093.7, 12 (Application Process pending) 05 (2022).
18. M. Kerbstadt, E. M. H. White, and M. C. Galetz, *Materials* **16**, 7480 (2023).
19. Available online: www.hb-specialalloy.com/products/rene-80/ (Accessed 22 March 2024).
20. J. Sumner, A. Potter, N. J. Simms, et al., *Materials at High Temperatures* **32**, 177 (2015).
21. T. König, X. Montero, and M. C. Galetz, *Materials and Corrosion* **70**, 1371 (2019).
22. X. Montero, A. Ishida, T. M. Meißner, H. Murakami, et al., *Corrosion Science* **166**, 108472 (2020).
23. D. Fähsing, C. Oskay, T. M. Meißner, et al., *Surface and Coatings Technology* **354**, 46 (2018).
24. C. Oskay, T. M. Meißner, C. Dobler, et al., *Coatings* **10**, 687 (2019).
25. D. Fähsing, Neuartige diffusions schichten zum oxidations schutz ferritisch-martensitischer Stähle in wasserdampfhaltigen Atmosphären. Shaker Verlag, PhD Thesis (2016).
26. M. A. Harper, R. A. Rapp, Chromized/siliconized pack cementation diffusion coatings for heat-resistant alloys, in Proceedings of the First International Conference on Heat Resistant Materials, eds. K. Natesan and D. J. Tillack, D.J. The American Society for Metals: Detroit (MI, USA, 1991), p. 379.
27. J. Safari and S. Nategh, *Journal of Materials Processing Technology* **176**, 240 (2006).
28. S. Gao, J. S. Hou, K. X. Dong, et al., *Acta Metallurgica Sinica* **30**, 261 (2017).
29. I. Gurrappa, *Materials Science and Technology* **19**, 178 (2003).
30. R. A. Rapp, *Corrosion Science* **44**, 209 (2002).
31. K. R. Peters, D. P. Whittle, and J. Stringer, *Corrosion Science* **16**, 791 (1976).
32. N. Eliaz, G. Shemesh, and R. M. Latanision, *Engineering Failure Analysis* **9**, 31 (2002).
33. D. J. Young, *High Temperature Oxidation and Corrosion of Metals*, (Elsevir, Amsterdam, 2008).
34. A. Jalowicka, et al., *Materials and Corrosion* **65**, 178 (2014).
35. F. H. Stott, F. I. Wei, and C. A. Enahoro, *Materials and Corrosion* **40**, 198 (1989).
36. M. Wambach, P. Ziolkowski, E. Müller, and A. Ludwig, *ACS Combinatorial Science* **21**, 362 (2019).
37. F. Fatemi and F. S. Nogorani, *Corrosion Science* **196**, 110031 (2022).
38. D. L. Douglass and J. S. Armijo, *Oxidation of Metals* **2**, 207 (1970).
39. C. E. Lowell, *Oxidation of Metals* **2**, 95 (1973).
40. C. Wagner, *JoES* **103**, 627 (1956).
41. M. A. Harper and R. A. Rapp, *Oxidation of Metals* **42**, 303 (1994).
42. S. Sheybany and D. L. Douglass, *Oxidation of Metals* **29**, 307 (1988).
43. M. F. Stroosnijder and W. J. Quadakkers, *High Temperature Technology* **4**, 41 (1986).
44. G. R. Johnston, *High Pressures* **14**, 695 (1982).